



Structural snapshot of a glycoside hydrolase family 8 endo- β -1,4-glucanase capturing the state after cleavage of the scissile bond

Takaaki Fujiwara,^a Ayumi Fujishima,^b Yui Nakamura,^b Kenji Tajima^c and Min Yao^{a,b,*}

Received 24 August 2021
 Accepted 3 December 2021

Edited by G. Kurisu, Osaka University, Japan

Keywords: bacterial cellulose; crystal structure; intermediates; hydrolysis; BcsZ; endo- β -1,4-glucanase.

PDB references: *EbBcsZ* bound to glycerol, 7f81; *EbBcsZ* bound to cellooligosaccharide, 7f82

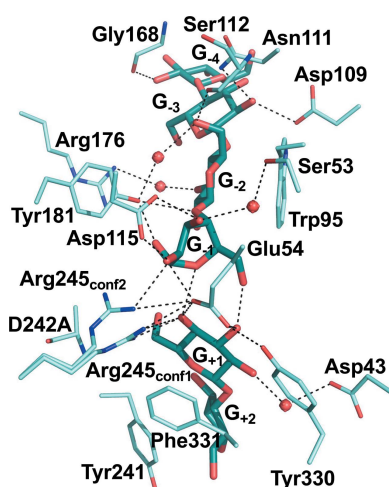
Supporting information: this article has supporting information at journals.iucr.org/d

^aFaculty of Advanced Life Science, Hokkaido University, Kita-10, Nishi-8, Kita-ku, Sapporo 060-0180, Japan, ^bGraduate School of Life Science, Hokkaido University, Kita-10, Nishi-8, Kita-ku, Sapporo 060-0180, Japan, and ^cFaculty of Engineering, Hokkaido University, Kita-13, Nishi-8, Kita-ku, Sapporo 060-8628, Japan. *Correspondence e-mail: yao@castor.sci.hokudai.ac.jp

Bacterial cellulose (BC), which is produced by bacteria, is a biodegradable and biocompatible natural resource. Because of its remarkable physicochemical properties, BC has attracted attention for the development and manufacture of biomedical and industrial materials. In the BC production system, the enzyme endo- β -1,4-glucanase, which belongs to glycoside hydrolase family 8 (GH8), acts as a cleaner by trimming disordered cellulose fibers to produce high-quality BC. Understanding the molecular mechanism of the endo- β -1,4-glucanase would help in developing a reasonable biosynthesis of BC. Nevertheless, all of the steps in the reaction of this endo- β -1,4-glucanase are not clear. This study confirms the BC hydrolytic activity of the endo- β -1,4-glucanase from the BC-producing bacterium *Enterobacter* sp. CJF-002 (*EbBcsZ*) and reports crystal structures of *EbBcsZ*. Unlike in previously reported GH8 endo- β -1,4-glucanase structures, here the base catalyst was mutated (D242A) and the structure of this mutant bound to cellooligosaccharide [*EbBcsZ*(D242A)_{CPT}] was analyzed. The *EbBcsZ*(D242A)_{CPT} structure showed two cellooligosaccharides individually bound to the plus and minus subsites of *EbBcsZ*. The glucosyl unit in subsite -1 presented a distorted ⁵S₁ conformation, a novel snapshot of a state immediately after scissile-bond cleavage. In combination with previous studies, the reaction process of endo- β -1,4-glucanase is described and the β -1,4-glucan-trimming mechanism of *EbBcsZ* is proposed. The *EbBcsZ*(D242A)_{CPT} structure also showed an additional β -1,4-glucan binding site on the *EbBcsZ* surface, which may help to accept the substrate.

1. Introduction

Worldwide, cellulose (β -1,4-glucan) production mainly relies on plants, but some bacteria can also produce a type of cellulose named bacterial cellulose (BC; Somerville, 2006; Ross *et al.*, 1991). Cellulose-producing bacteria secrete BC as an exopolysaccharide, forming a hierarchical assembly outside the cell. Unlike the lignocellulosic matrix derived from plant cell walls, BC displays a naturally high purity and high crystallinity (Chundawat *et al.*, 2011; Czaja *et al.*, 2004). BC also has high mechanical strength (Yamanaka *et al.*, 1989), biodegradability (Torgbo & Sukyai, 2020) and biocompatibility (Helenius *et al.*, 2006). These unique characteristics make BC an attractive environmentally friendly resource for the development and manufacture of biomedical or industrial materials such as wound dressings (Czaja *et al.*, 2006), artificial blood vessels (Lee & Park, 2017), electronic paper displays (Nogi & Yano, 2008; Shah & Brown, 2005) and speaker diaphragms (Nishi *et al.*, 1990). Despite numerous efforts to



improve BC production (Lee *et al.*, 2014), such as optimization of the composition of culture media, bioreactors and bacterial strains, bacteria do not satisfy the demand for BC. Understanding the mechanism of BC biosynthesis will therefore help to produce BC more efficiently, and has become a hot topic in BC research.

Cellulose-producing bacteria biosynthesize BC using a multi-protein complex (terminal complex; TC) localized on the outer and inner membranes. *Komagataeibacter xylinus* (formerly called *Acetobacter xylinum*) serves as a model bacterium for BC biosynthesis. In *K. xylinus*, the TC is composed of BC synthase subunits A, B, C and D (BcsA, BcsB, BcsC and BcsD, or alternatively BcsAB, BcsC and BcsD; Kawano *et al.*, 2002; Wong *et al.*, 1990). Analyzing the individual structures of the subunits clarified their roles in BC biosynthesis (Acheson *et al.*, 2019; Nojima *et al.*, 2017; Fujiwara *et al.*, 2013; Morgan *et al.*, 2013, 2016; Hu *et al.*, 2010). The production of high-quality BC depends on both the TC and some accessory factors such as cleaner proteins. The *cmcax* gene, which is located upstream of the BC synthase operon in *K. xylinus*, encodes CMCax, an endo- β -1,4-glucanase (EC 3.2.1.4) that hydrolyzes carboxymethyl cellulose (CMC) and cellooligosaccharides (Yasutake *et al.*, 2006; Standal *et al.*, 1994). Disruption of the *cmcax* gene reduced the amount of BC produced (Nakai *et al.*, 2013), while overexpression of CMCax increased it (Kawano *et al.*, 2008). Furthermore, adding a CMCax antibody to the culture medium inhibited the formation of BC fibers (Koo *et al.*, 1998). Considering the hydrolytic activity of CMCax, endo- β -1,4-glucanase could act as a cleaner protein to produce high-quality BC by trimming disordered cellulose. Interestingly, BcsZ, an endo- β -1,4-glucanase encoded in the BC synthase operon, also exists in most bacterial lineages (Römling & Galperin, 2015). Recent studies showed that *Enterobacter* sp. CJF-002, isolated from rocks in oil reservoirs, efficiently produces BC and is a promising bacterium for producing large amounts of BC (Sunagawa *et al.*, 2012). In *Enterobacter* sp. CJF-002, a single operon encodes BcsA, BcsB, BcsZ and BcsC. Although CMCax and BcsZ have low sequence similarity (19% identity), the residues located in the catalytic site are highly conserved (Supplementary Fig. S1). BcsZ from *Enterobacter* sp. CJF-002 (*EbBcsZ*; GenBank accession No. BAM44856) and cellulolytic *Escherichia coli* (*EcBcsZ*) also hydrolyze cellooligosaccharides and CMC (Pang *et al.*, 2019; Sunagawa *et al.*, 2012; Mazur & Zimmer, 2011), indicating that BcsZ and CMCax are functionally homologous. Therefore, a biological function of *EcBcsZ* could be to promote the formation of cellulose fibers by degrading β -1,4-glucan chains (Mazur & Zimmer, 2011).

Similar to endo- β -1,4-xylanases (EC 3.2.1.8), licheninases (EC 3.2.1.73), chitosanases (EC 3.2.1.132) and reducing-end xylose-releasing exo-oligoxylanases (EC 3.2.1.156), CMCax and BcsZ belong to glycoside hydrolase family 8 (GH8; CAZy; <http://www.cazy.org>). The catalytic reaction of GH8 enzymes is a single-displacement mechanism accompanied by an inversion of the anomeric configuration of the sugar unit in subsite -1 , which changes the conformation of pyranose from β - 4C_1 to α - 4C_1 (Koshland, 1953; Cremer & Pople, 1975; Fig. 1, Supplementary Fig. S1). The general acid catalyst donates a proton to the C1 atom to release the hemiacetal sugar. The general base catalyst activates a water molecule for a nucleophilic attack on the anomeric center (C1) of the substrate. Displacement of the activated water molecule and liberation of the leaving group of the product occur on the C1 atom of a distorted oxocarbenium ion intermediate, forming an α -configuration at the C1 atom. To understand the reaction mechanism of GH8 enzymes, structures of GH8 enzymes and their acid catalyst mutants bound to oligosaccharides have been analyzed to date. In the structure of the E55Q mutant of *EcBcsZ* bound to cellopentaose (CPT) [*EcBcsZ*(E55Q)_{CPT}; PDB entry 3qxl], the glucosyl unit in subsite -1 (G_{-1}) presented an α - 4C_1 conformation, showing that *EcBcsZ* (E55Q)_{CPT} is the product-binding form (Mazur & Zimmer, 2011). In contrast, the structure of the E95Q mutant of *CtCelA* from *Clostridium thermocellum* bound to CPT [*CtCelA* (E95Q)_{CPT}; PDB entry 1kwf] showed that G_{-1} presented a $^{2,5}B$ conformation and thus *CtCelA*(E95Q)_{CPT} was an intermediate in the transition state (Guérin *et al.*, 2002). Interestingly, the structure of wild-type endo- β -1,4-xylanase from *Teredinibacter turnerae* bound to xylotriose (XTO) (*TtGH8*_{XTO}; PDB entry 6g0b) confirmed the existence of a $^{2,5}B$ conformation of the xylosyl unit in subsite -1 (X_{-1} ; Fowler *et al.*, 2018). Based

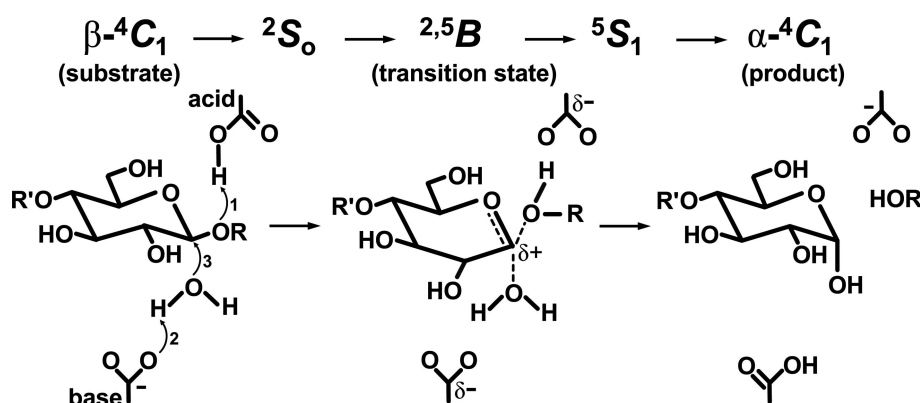


Figure 1

General reaction mechanism of inverting glycoside hydrolases. The upper part shows the proposed conformational changes of the sugar in subsite -1 (G_{-1}). β - 4C_1 , $^{2,5}B$ and α - 4C_1 are the conformations of G_{-1} in the substrate, oxocarbenium ion intermediate (transition state) and product, respectively. 2S_0 and 5S_1 are the conformations of the other intermediates. The lower part shows the proposed catalytic process of GH8 enzymes. The reaction follows the single-displacement mechanism through the oxocarbenium ion intermediate. The numbers in the left part represent the order of the displacement reaction, *i.e.* protonation of the glycosidic bond occurs followed by nucleophilic attack of an activated water molecule. G_{-1} is shown as a six-membered sugar. The substrate, transition intermediate and product are shown in the left, middle and right panels, respectively. Before and after forming the oxocarbenium intermediate, G_{-1} forms 2S_0 and 5S_1 conformations, respectively.

on these structures, a computational simulation predicted that in the reaction process of GH8 enzymes the G_{-1} conformational change sequence was $\beta\text{-}^4C_1 \rightarrow \text{}^2S_O \rightarrow \text{}^{2,5}B \rightarrow \text{}^5S_1 \rightarrow \alpha\text{-}^4C_1$ (Ardèvol & Rovira, 2015; Petersen *et al.*, 2009; Fig. 1). However, the coordinates of the $\text{}^2S_O$ and $\text{}^5S_1$ intermediates remain unclear since no structural data are available to prove the existence of such intermediates of GH8 enzymes.

In this study, we assessed the hydrolytic activity of *EbBcsZ* on BC produced by *K. xylinus*. Based on the idea that BcsZ hydrolyzes cellulose through an inverting mechanism, we mutated the base catalyst Asp242 to alanine (D242A) and determined the structure of this mutant in complex with a celooligosaccharide [*EbBcsZ*(D242A)_{CPT}]. The *EbBcsZ*(D242A)_{CPT} structure showed a novel snapshot of a reaction stage immediately after scissile-bond cleavage. It displayed a distorted $\text{}^5S_1$ conformation of G_{-1} . Moreover, the structure of wild-type *EbBcsZ* in complex with glycerol (*EbBcsZ*_{GOL}) supported the existence of the $\text{}^5S_1$ conformation in the reaction process of BcsZ. We finally compared our structures with those of other GH8 endo- β -1,4-glucanases, extended the previously described reaction mechanism of GH8 enzymes and proposed a β -1,4-glucan-trimming mechanism for *EbBcsZ*.

2. Materials and methods

2.1. Cloning, expression and purification

Except for the N-terminal signal peptide (Met1–Ala20), we amplified the gene fragment encoding *EbBcsZ* (amino acids Ala21–Gln367) by PCR using the genome of *Enterobacter* sp. CJF-002 as a template using the primers 5'-GGAATTCCA TATGGCCTGCACATGGCCTGC-3' and 5'-CCGCTCGAG TTACTGTGAACTTGCGCATGCCTG-3'. We used NdeI and XhoI to digest the amplified gene fragments and the protein expression vector pET-28b (Novagen) with a hexahistidine tag and thrombin cleavage sequence at the N-terminus, and then ligated them. We transformed the expression plasmids into *E. coli* strain BL21(DE3) by electroporation. We grew the cells in LB medium supplemented with 25 $\mu\text{g ml}^{-1}$ kanamycin at 37°C until the OD₆₀₀ reached 0.5. We then induced overexpression of recombinant *EbBcsZ* by adding 100 μM isopropyl β -D-1-thiogalactopyranoside to the culture medium and cultured the cells overnight at 25°C. After resuspending the harvested cells in buffer A [50 mM HEPES–KOH buffer pH 8.0 containing 500 mM potassium chloride and 10% (v/v) glycerol], we lysed the cells by sonication. We centrifuged the cell lysate at 40 000g for 15 min at 10°C and then loaded the supernatant onto a nickel-affinity chromatography column (5 ml HisTrap HP; Cytiva) equilibrated with buffer A. We then eluted the bound *EbBcsZ* with buffer B [50 mM HEPES–KOH buffer pH 8.0 containing 500 mM potassium chloride, 10% (v/v) glycerol and 500 mM imidazole] in a linear gradient of imidazole from 50 to 500 mM. We collected the eluate containing *EbBcsZ* and then removed the N-terminal hexahistidine tag using thrombin (Fujifilm Wako) overnight at 4°C. We then again loaded

EbBcsZ onto a nickel-affinity chromatography column and collected the eluate containing the protein, which had lost its affinity for the column. Finally, we purified *EbBcsZ* on a Superdex 200 16/600 column (Cytiva) equilibrated with buffer C (50 mM HEPES–KOH buffer pH 8.0 containing 150 mM potassium chloride). We introduced the D242A mutation using the designed primers by the QuikChange technique and confirmed it by sequencing. We prepared the *EbBcsZ*(D242A) mutant as described above for wild-type *EbBcsZ*. We concentrated the purified *EbBcsZ* and *EbBcsZ*(D242A) to a final concentration of 9 mg ml⁻¹ by ultrafiltration using Vivaspin 6 concentrators with a 10 kDa cutoff membrane (Cytiva).

2.2. Crystallization and X-ray diffraction data collection

We performed initial crystallization screening for both proteins using sparse-matrix crystallization kits from Qiagen, Hilden, Germany. We mixed 0.5 μl protein solution with an equal volume of reservoir solution and used the sitting-drop vapor-diffusion method. We obtained *EbBcsZ* and *EbBcsZ*(D242A) crystals using the same reservoir solution consisting of 0.2 M disodium tartrate, 20% (w/v) PEG 3350. Crystals grew to dimensions of 0.3 \times 0.2 \times 0.2 mm within three days at 20°C. We transferred the *EbBcsZ*(D242A) crystals into soaking solution [0.2 M disodium tartrate, 20% (v/v) PEG 3350, 20% (v/v) glycerol, 2 mM CPT] and incubated them for 20 h at 20°C. We soaked the *EbBcsZ* crystals in reservoir solution supplemented with 20% (v/v) glycerol and then flash-cooled both crystals under a stream of liquid nitrogen. We collected diffraction data on beamlines NW-12A at Photon Factory, Tsukuba, Japan and BL41XU at SPring-8, Hyogo, Japan and processed the data using XDS (Kabsch, 2010). Table 1 summarizes the data statistics.

2.3. Structure determination and refinement

To determine the structure of *EbBcsZ* in complex with glycerol (*EbBcsZ*_{GOL}), we used the molecular-replacement (MR) method with *AutoMR* from the *Phenix* package (Liebschner *et al.*, 2019) using the *EcBcsZ*_{apo} structure (PDB entry 3qxf; Mazur & Zimmer, 2011) as the search model. We calculated the rotation and translation functions using data in the resolution range 45.0–3.0 Å. Similarly, we determined the *EbBcsZ*(D242A)_{CPT} structure by the MR method with *AutoMR* using the *EbBcsZ*_{GOL} structure as the search model. We calculated rotation and translation functions using data in the resolution range 45.0–2.5 Å. We performed several rounds of refinement using *phenix.refine* from the *Phenix* suite, alternating with manual fitting and rebuilding based on $2F_o - F_c$ and $F_o - F_c$ electron-density maps using *Coot* (Emsley *et al.*, 2010). We confirmed the conformation of the β -1,4-glucan chains based on the omit map. Table 1 summarizes the final refinement statistics and geometry defined by *MolProbity* (Chen *et al.*, 2010). We prepared the structural figures using *PyMOL* (<http://www.pymol.org>).

2.4. BC hydrolysis assay

To perform the BC hydrolysis assay, we cultured *K. xylinus* to obtain BC based on the method reported previously (Czaja *et al.*, 2004). BC is porous and incorporates water molecules, forming a gelatinous structure. To reduce the variation in the produced BC, we collected BC from a cultured medium as follows. We placed *K. xylinus* cells into 5 ml Schramm–Hestrin (HS) medium (Schramm & Hestrin, 1954) and initially grew them at 30°C with stirring at 170 rev min⁻¹ for four days. We then inoculated 0.1 ml cultured medium into 3 ml fresh HS medium and grew the cells at 30°C with stirring at 120 rev min⁻¹ for three days. The dry mass of BC was referenced each time to control the amount of produced BC. We collected the gelatinous BC membrane and gently washed it with 3 ml buffer *D* (50 mM sodium citrate buffer pH 5.0 containing 200 mM sodium chloride). To measure BC hydrolysis, the solution containing the purified *EbBcsZ* and *EbBcsZ*(D242A) was changed to buffer *D*. We performed repetitive concentration and dilution of purified *EbBcsZ* and *EbBcsZ*(D242A) by ultrafiltration using Vivaspin 6 concentrators with a 10 kDa cutoff membrane, and finally adjusted the concentration of the samples to 10 mg ml⁻¹. We dissolved bovine serum albumin (BSA; Sigma–Aldrich) and cellulase ONOZUKA RS (Yakult Pharmaceutical Industry) in buffer *D* to a concentration of 10 mg ml⁻¹ as negative and positive controls, respectively. We transferred the prepared gelatinous membrane of BC into 3 ml of each enzyme solution and incubated the mixtures at 30°C with stirring at 170 rev min⁻¹ for 20 h. Since the turbidity of the BC solution increases as BC

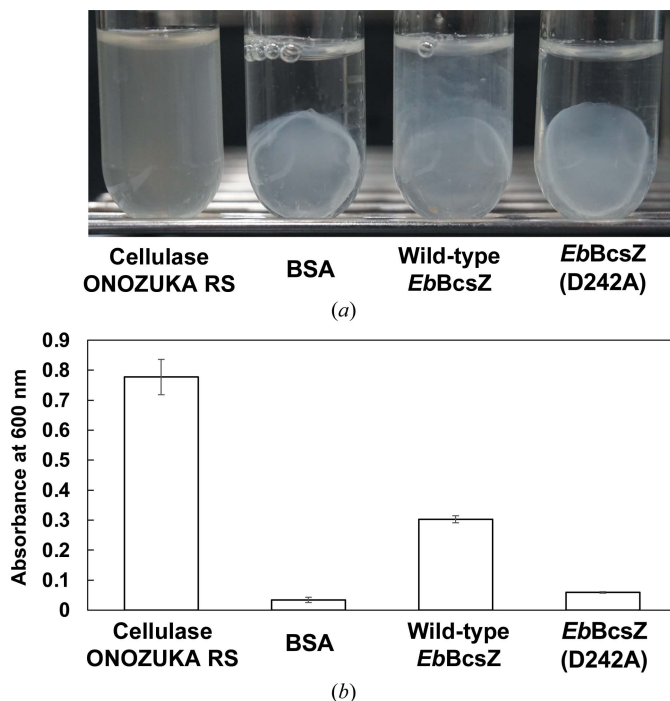


Figure 2 BC hydrolysis assay for *EbBcsZ*. (a) The state of gelatinous BC after 20 h of incubation with cellulase ONOZUKA RS, bovine serum albumin (BSA), *EbBcsZ* and *EbBcsZ*(D242A). (b) Turbidity of the assay solution measured after 20 h of incubation. Average and standard deviation values of the absorbance at 600 nm were calculated from four replicates ($N = 4$).

Table 1

Data-collection and refinement statistics.

Values in parentheses are for the highest resolution shell.

	<i>EbBcsZ</i> (D242A) _{CPT}	<i>EbBcsZ</i> _{GOL}
Data collection		
Wavelength (Å)	1.0000	1.0000
Space group	$P2_1$	$P2_1$
a, b, c (Å)	89.3, 92.9, 90.5	89.3, 91.5, 89.9
α, β, γ (°)	90, 98.4, 90	90, 98.2, 90
Resolution (Å)	50.0–1.30 (1.38–1.30)	50.0–1.93 (2.05–1.93)
R_{merge}^\dagger	0.030 (0.567)	0.063 (0.597)
Multiplicity	4.2 (3.5)	3.8 (3.8)
Completeness (%)	99.5 (98.8)	99.7 (99.3)
No. of unique reflections	355775 (57751)	107156 (17177)
Mean $I/\sigma(I)$	21.4 (2.3)	18.3 (2.6)
$CC_{1/2}$	1.000 (0.873)	0.999 (0.837)
Refinement		
Resolution (Å)	42.51–1.30	38.34–1.93
$R_{\text{work}}^\ddagger/R_{\text{free}}^\S$	0.169/0.187	0.162/0.197
No. of atoms		
Protein	10990	10876
Water	1179	957
Cellooligosaccharide	329	—
Glycerol	—	126
Disodium tartrate	20	20
R.m.s.d.s		
Bond lengths (Å)	0.014	0.009
Bond angles (°)	1.573	0.952
Ramachandran statistics (%)		
Favored	98.59	98.51
Allowed	1.41	1.49
Outliers	0	0
Mean B factors (Å ²)		
Protein	24.57	30.69
Water	33.01	38.22
Cellooligosaccharide	32.26	—
Glycerol	—	38.99
Disodium tartrate	22.11	26.78
PDB code	7f82	7f81

[†] $R_{\text{merge}} = \frac{\sum_{hkl} \sum_i |I_i(hkl) - \langle I(hkl) \rangle|}{\sum_{hkl} \sum_i I_i(hkl)}$, where i is the number of observations of a given reflection and $\langle I(hkl) \rangle$ is the average intensity of the i observations. [‡] $R_{\text{work}} = \frac{\sum_{hkl} |F_{\text{obs}}| - |F_{\text{calc}}|}{\sum_{hkl} |F_{\text{obs}}|}$. [§] R_{free} was calculated using a randomly selected 5% of reflections that were excluded from refinement.

is hydrolyzed, we observed the turbidity of each enzyme solution to estimate the BC hydrolysis. Finally, we measured the absorbance of each sample at 600 nm. We performed four technical replicates for each condition.

3. Results

3.1. The hydrolytic activity of *EbBcsZ* towards BC

Like CMCax, *EbBcsZ* can hydrolyze cellooligosaccharides, including cellopentaose, celohexaose and CMC, an aqueous cellulose derivative (Nakai *et al.*, 2013; Mazur & Zimmer, 2011). To investigate whether *EbBcsZ* acts on gelatinous BC, we performed a hydrolysis assay on BC produced by *K. xylinus*. To estimate the degree of BC hydrolysis, we measured the absorbance at 600 nm representing the turbidity of BC-containing solutions in the presence or absence of *EbBcsZ*. In the positive control, BC hydrolysis allowed the cells embedded in gelatinous BC to disperse into the solution, increasing the turbidity (Fig. 2, left). Incubating the BC-containing solution with wild-type *EbBcsZ* partly degraded

gelatinous BC (Fig. 2*a*). The turbidity of this solution was 40% of that of the positive control (Fig. 2*b*), indicating that *EbBcsZ* has a moderate hydrolytic activity on BC. In contrast, the base catalyst mutant *EbBcsZ*(D242A) barely changed the shape of gelatinous BC (Fig. 2*a*, right), and the turbidity of the BC solution incubated with *EbBcsZ*(D242A) was comparable to that of the negative control (Fig. 2*b*, right).

3.2. The structure of *EbBcsZ* in complex with cellooligosaccharide

Similar to the homologous enzyme *EcBcsZ* (Mazur & Zimmer, 2011), we prepared *EbBcsZ* without the N-terminal signal peptide (Met1–Ala20) and with a mutation of the base catalyst (D242A) to elucidate the reaction mechanism of *EbBcsZ*. We determined the structure of *EbBcsZ*(D242A)_{CPT} at 1.30 Å resolution by soaking *EbBcsZ*(D242A) crystals in a

solution containing CPT. In this *EbBcsZ*(D242A)_{CPT} structure, the residues Cys22–Trp359 were visible, while the N-terminal Ala21 and the eight C-terminal residues (Gly360–Gln367) could not be built due to poor electron density. The overall structure of *EbBcsZ*(D242A)_{CPT} formed a classical (α/α)₆ barrel composed of six inner and lateral antiparallel helices. Although *EbBcsZ* is a monomeric enzyme, the asymmetric unit contained four *EbBcsZ*(D242A)_{CPT} monomers. These four monomers were essentially identical, with a root-mean-square deviation (r.m.s.d.) value of less than 0.41 Å for 335 C α atoms. We selected monomer *A* for structural comparison and description of the active site. Structural comparison using *PDBeFold* (Krissinel & Henrick, 2004) showed that *EbBcsZ*(D242A)_{CPT} was similar to the other GH8 endo- β -1,4-glucanases *EcBcsZ*(E55Q)_{CPT} (PDB entry 3qxq), *CtCelA*(E95Q)_{CPT} (PDB entry 1kwf) and CMCax (PDB entry 1wzz), with r.m.s.d.s of 0.65 Å for 338 C α atoms, 2.09 Å for 270 C α atoms and 2.02 Å for 278 C α atoms, respectively. Although we soaked the crystals in a CPT-containing solution, we did not obtain full-length CPT in the *EbBcsZ*(D242A)_{CPT} structure, unlike in the *EcBcsZ*(E55Q)_{CPT} and *CtCelA*(E95Q)_{CPT} structures. In each monomer of the asymmetric unit, two cellooligosaccharides occupied the plus and minus subsites (both sides of the cleavage position) of the active site (Fig. 3*a*, Supplementary Fig. S3), indicating an intermediate state that differs from those of reported GH8 endo- β -1,4-glucanase structures. In all four monomers, cellobiose binds to subsites +1 to +2 similarly, whereas the cellooligosaccharide binds to the minus subsites differently. Cellotetraose bound to subsites –1 to –3 and extended to an additional subsite –4 in three monomers (monomers *A*–*C*), while cello-triose bound to subsites –2 to –4 in the remaining monomer (monomer *D*) (Fig. 3*a*).

We next compared the *EbBcsZ*(D242A)_{CPT} structure with those of other GH8 endo- β -1,4-glucanases. The cellobiose orientation in subsites +1 to +2 of *EbBcsZ*(D242A)_{CPT} was similar to that of *CtCelA*(E95Q)_{CPT} (Guérin *et al.*, 2002). G₊₁ and G₊₂ formed stacking interactions with the aromatic residues in the same manner. However, there were differences in the interaction between the hydroxy group of G₊₁ and polar residues in the structures of both *EbBcsZ*(D242A)_{CPT} and *CtCelA*(E55Q)_{CPT} (Fig. 3*b*). Note that in the *EbBcsZ*(D242A)_{CPT} structure the

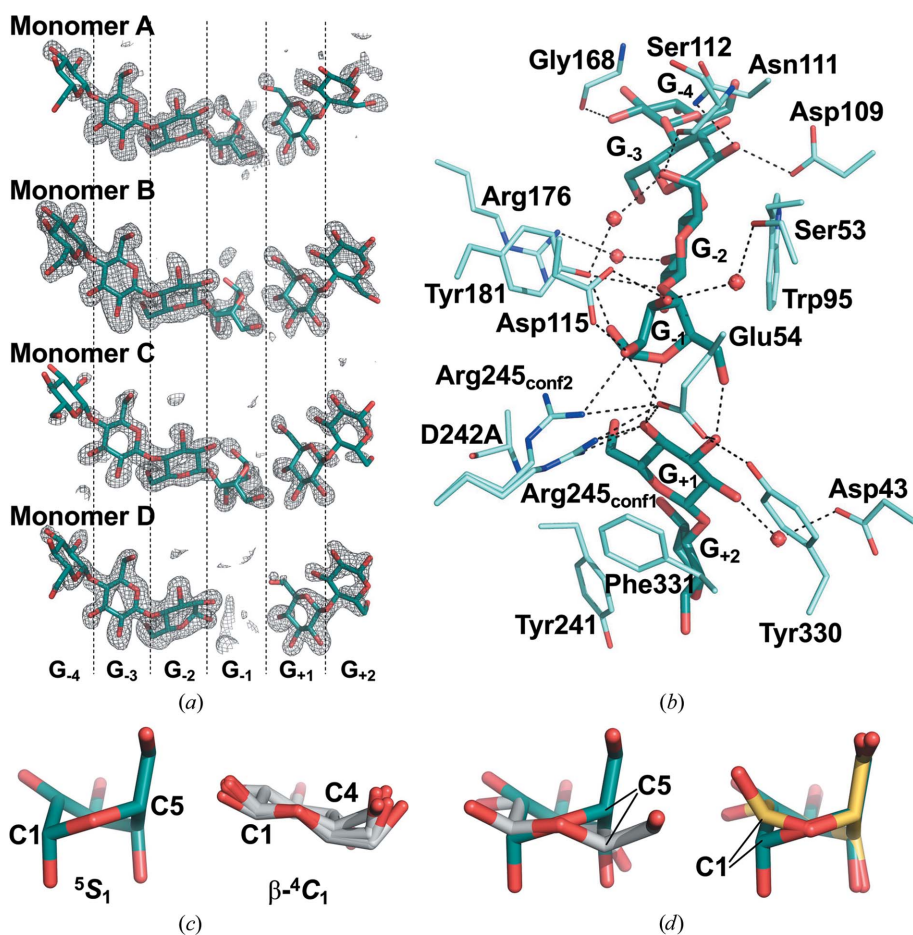


Figure 3
The structure of the active site in *EbBcsZ*(D242A)_{CPT}. (*a*) Electron densities of the β -1,4-glucan chains bound to the four monomers of the asymmetric unit. The electron densities are the omit map contoured at 3.0 σ . (*b*) Interactions between the β -1,4-glucan chains and the residues in the active site. We selected monomer *A* as the representative active site. The water molecules and the residues interacting with the β -1,4-glucan chains are represented as red spheres and light blue lines, respectively. The hydrogen-bond network is represented as dotted lines. In (*a*) and (*b*), the β -1,4-glucan chains are shown as sticks and O, N and C atoms are shown in red, blue and dark cyan, respectively. (*c*) The conformation of G₋₁ (dark cyan) and five other glucosyl units in subsites G₋₂, G₋₃, G₋₄, G₊₁ and G₊₂ (light gray) of *EbBcsZ*(D242A)_{CPT}. (*d*) Superposed views of glucosyl units. Left: superposition of G₋₁ (dark cyan) and G₋₂ (light gray) in *EbBcsZ*(D242A)_{CPT}. Right: superposition of G₋₁ in *EbBcsZ*(D242A)_{CPT} (dark cyan) and G₋₁ in *CtCelA*(E95Q)_{CPT} (yellow).

Arg245 side chain presented two different conformations (Arg245_{conf1} and Arg245_{conf2}). The Arg245_{conf1} side chain interacts with the 4-OH of G₊₁. Additionally, the side chain of the general acid catalyst Glu54, corresponding to E95Q in *CtCelA* and E55Q in *EcBcsZ*, interacted with the 3-OH and 4-OH of G₊₁. Our structure also displayed an interaction network associated with Glu54. Glu54 interacts with Arg245 and Tyr330 through a salt bridge and a hydrogen bond, respectively. Except for G₋₁, four glucosyl units interacted with the minus subsites in the same manner as those in *EcBcsZ*(E55Q)_{CPT} and *CtCelA*(E95Q)_{CPT} (Mazur & Zimmer, 2011; Guérin *et al.*, 2002). In *EbBcsZ*(D242A)_{CPT}, the Asp115 side chains formed a bidentate interaction with G₋₁, and the Glu54 side chain interacted with the 2-OH of G₋₁. Furthermore, we observed an interaction between G₋₁ and G₊₁ in the *EbBcsZ*(D242A)_{CPT} structure. The 6-OH and sugar-ring O (O5) atoms of G₋₁ interacted with the 3-OH and 4-OH of G₊₁, respectively, through hydrogen bonds.

3.3. The glucosyl unit conformation in subsite -1

In the *EbBcsZ*(D242A)_{CPT} structure, G₋₁ displayed a distorted ⁵S₁ conformation, whereas the glucosyl units in the other subsites (G₋₂, G₋₃, G₋₄, G₊₁ and G₊₂) presented a stable β -⁴C₁ chair conformation (Fig. 3c, Supplementary Table

S1). Moreover, considering the position of the 1-OH of G₋₁, G₋₁ has the α -configuration at the C1 atom. Comparing the C5 position of G₋₁ with those of the other glucosyl units clearly shows this difference (Fig. 3d, left). G₋₁ displayed a ^{2,5}B conformation in the *CtCelA*(E95Q)_{CPT} structure, and comparing the C1 positions of G₋₁ in *EbBcsZ*(D242A)_{CPT} and *CtCelA*(E95Q)_{CPT} also shows the difference in the conformation of G₋₁ (Fig. 3d, right). To confirm whether the alanine mutation of the general base catalyst Asp242 causes structural changes, we determined the structure of *EbBcsZ* in complex with glycerol (*EbBcsZ*_{GOL}). We obtained *EbBcsZ* crystals in the same crystal form as those of *EbBcsZ*(D242A)_{CPT}. Residues Cys22–Trp359 of each *EbBcsZ*_{GOL} monomer were built in the asymmetric unit. *EbBcsZ*_{GOL} and *EbBcsZ*(D242A)_{CPT} had very similar structures, with an r.m.s.d. of 0.17 Å for 335 C α atoms, demonstrating that the D242A mutation scarcely changed the overall *EbBcsZ* structure. In the *EbBcsZ*_{GOL} structure, subsites -1, -2 and +1 were occupied by glycerol molecules used as a cryoprotectant for the diffraction experiment (Supplementary Fig. S4a). These glycerol molecules can be considered to be a mimic of the bound glucosyl unit of β -1,4-glucan. In each *EbBcsZ* monomer the glycerol molecule in subsite -1 adopted a remarkably similar orientation. Superposing *EbBcsZ*_{GOL} on *EbBcsZ*(D242A)_{CPT} showed that three hydroxy groups of the glycerol and two water molecules were close to the O5 atom and 3-OH, 6-OH, 1-OH and 2-OH of G₋₁, respectively (Supplementary Fig. S4b, Supplementary Table S2), supporting the plausibility of the formation of a distorted ⁵S₁ conformation of G₋₁ during the hydrolytic reaction process. Besides, the existence of the ⁵S₁ conformation is consistent with the predicted result of a quantum mechanics/molecular mechanics (QM/MM) dynamic simulation on the reaction process of GH8 enzymes (Ardèvol & Rovira, 2015; Petersen *et al.*, 2009).

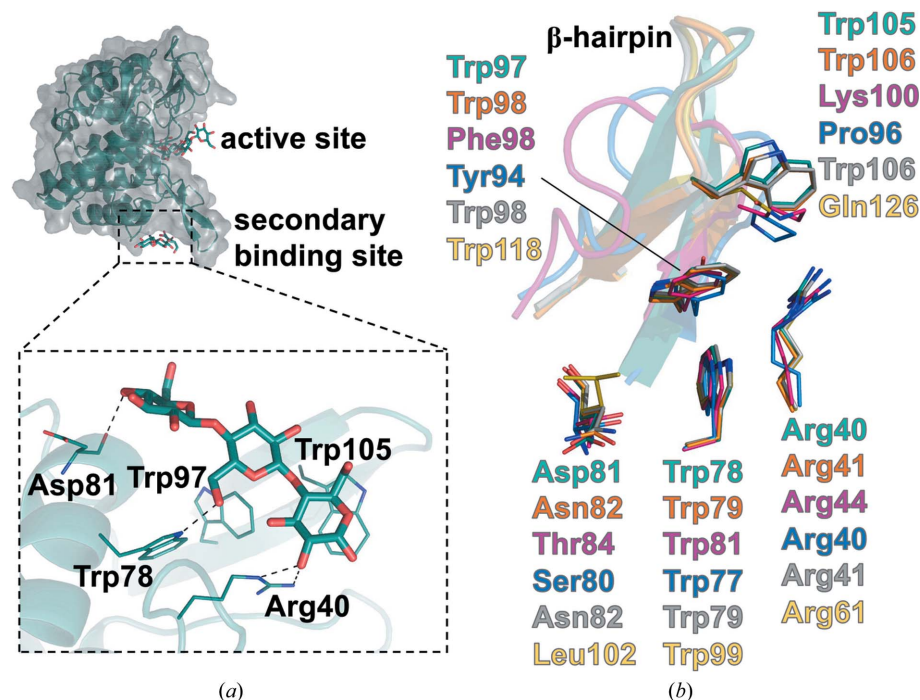


Figure 4

The structure of the secondary binding site in *EbBcsZ*(D242A)_{CPT}. (a) Close-up view of the secondary binding site. The cellotriose and the residues interacting with it are represented as sticks and lines, respectively. The hydrogen bonds between cellotriose and the residues of *EbBcsZ*(D242A)_{CPT} are represented as dotted lines. (b) Superposition of the residues interacting with cellotriose in *EbBcsZ* and the other endo- β -1,4-glucanases. The residues of *EbBcsZ*(D242A)_{CPT} (dark cyan), *EcBcsZ*(E55Q)_{CPT} (PDB entry 3qxq, orange), CMCax (PDB entry 1wzz, pink), Cel110 (PDB entry 5gy3, blue), BcsZ (PDB entry 4q2b, gray) and hydrolyase from *Vibrio fischeri* (PDB entry 5cd2, yellow) are labeled and represented as lines. The β -hairpin region of *EbBcsZ*(D242A)_{CPT} and the corresponding regions in the other endo- β -1,4-glucanases are represented as ribbons.

3.4. The secondary binding site of the β -1,4-glucan chain

Among the GH8 endo- β -1,4-glucanases, the structure of *EbBcsZ*(D242A)_{CPT} is the first to show that β -1,4-glucan binds to the surface away from the active site (Fig. 4a), which is called the secondary binding site (Cuyvers *et al.*, 2012). Two of the four *EbBcsZ*(D242A)_{CPT} monomers (monomers A and C) bind to cellotriose through a tryptophan-rich cleft (Fig. 4a). However, electron density for the cellooligosaccharide did not appear in the corresponding region in monomers

B and *D*, which can be considered to be an effect of crystal packing (Supplementary Fig. S5). This marked difference implies that the physical and chemical environment easily affects the binding of β -1,4-glucan at the secondary binding site. Cellotriose bound to monomers *A* and *C* in the same manner. The glucosyl units at the central part and the reducing end formed a T-shaped stacking with Trp97 and π - π stacking with Trp105, respectively. Stacking interactions with aromatic residues are common in secondary binding sites and seem to be essential for oligosaccharide binding (Cockburn *et al.*, 2016; Cockburn & Svensson, 2013; Cuyvers *et al.*, 2011). The 2-OH of the reducing-end sugar and the 6-OH of the central sugar interacted with the side chains of Arg40 and Trp78, respectively. The 4-OH of the non-reducing-end sugar interacted with the main-chain carbonyl of Asp81 through a hydrogen

bond. These contacts are probably conserved among the other GH8 endo- β -1,4-glucanases, except for the stacking with Trp105 in a β -hairpin motif (Fig. 4*b*).

4. Discussion

BC, which is generated by cellulose-producing bacteria, is a biomaterial with remarkable characteristics that are superior to those of the cellulose fiber extracted from plants. It has potential applications in various fields. In BC-producing bacteria, the endo- β -1,4-glucanase serves as a cleaner protein that degrades disordered cellulose fibers, efficiently producing high-quality BC. Our work is focused on investigating the structural and functional properties of the endo- β -1,4-glucanase BcsZ in order to help to improve BC production.

A BC degradation assay showed that *EbBcsZ* has hydrolytic activity, although it is weaker than that of cellulase ONOZUKA RS, a multi-component cellulase. This weak activity may arise from limited degradation of the disordered region in gelatinous BC, which is in agreement with previous studies showing that *EbBcsZ* can degrade cellooligosaccharides and CMC to noncrystalline cellulose (Koo *et al.*, 1998). Considering that the endo- β -1,4-glucanase *EbBcsZ* needs to access the β -1,4-glucan chain to cleave internal bonds, secondary binding sites probably assist in the binding of the target substrate β -1,4-glucan chain. Moreover, immunostaining of CMCax (Standal *et al.*, 1994) and digestion of BcsZ from *Salmonella typhimurium* by a protease (Ahmad *et al.*, 2016) demonstrated that these endo- β -1,4-glucanases are located close to the outer membrane or periplasmic space, allowing them to degrade β -1,4-glucan chains before crystallization (Ahmad *et al.*, 2016; Hu *et al.*, 2010; Standal *et al.*, 1994). A phylogenetic relationship shows that the gene encoding endo- β -1,4-glucanase appears with the *bcsC* gene in the *bcs* gene cluster, with some exceptions (Römling & Galperin, 2015). This little-studied BcsC subunit of TC localizes at the outer membrane and periplasmic space, and contributes to the export of BC to the extracellular matrix. Thus, endo- β -1,4-glucanase may be associated with BcsC to access noncrystalline β -1,4-glucan chains efficiently.

Several studies have reported structures of wild-type GH8 endo- β -1,4-glucanases and general acid catalyst mutants. These studies considered that the apo-form structures of these GH8 endo- β -1,4-glucanases represented the 'resting state'. Here, we select *EcBcsZ*_{apo} as representing the resting state (Fig. 5*a*, i) since it is most similar to *EbBcsZ* in both sequence and structure. In the structures of *CiCelA*(E95Q)_{CPT} (Guérin *et al.*, 2002) and *TiGH8*_{XTO} (Fowler *et al.*, 2018), a single oligosaccharide was incorporated into the subsites, and G₋₁ and X₋₁ showed a distorted ^{2,5}*B* conformation. These complex structures represent the 'reactive state' that readily forms the oxocarbenium intermediate (Fig. 5*a*, ii). In the *EcBcsZ*(E55Q)_{CPT} structure cellopentaose was only located in the minus subsites, meaning that *EcBcsZ*(E55Q)_{CPT} represents the 'post-hydrolysis state' that occurs after release of the leaving group (Fig. 5*a*, iv). We employed a base-catalyst mutant *EbBcsZ*(D242A) and determined its cellooligosaccharide-

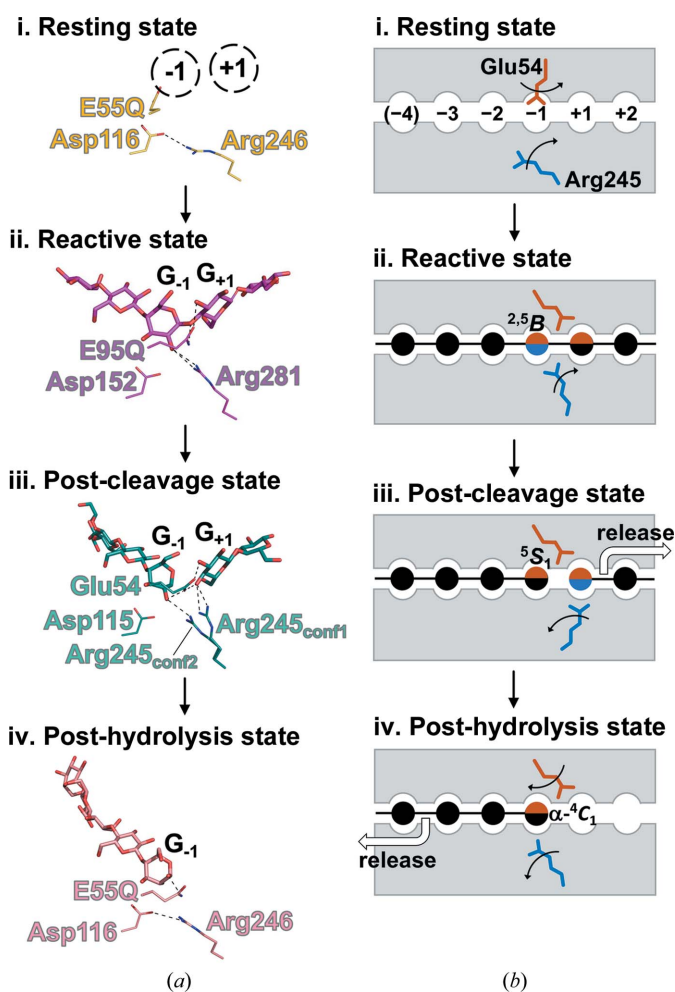


Figure 5 Interactions between the bound β -1,4-glucan chains and the polar residues of GH8 endo- β -1,4-glucanases in each reaction state. (a) The structures of (i) the resting state *EcBcsZ*_{apo}, (ii) the reactive state *CiCelA*(E95Q)_{CPT}, (iii) the post-cleavage state *EbBcsZ*(D242A)_{CPT} and (iv) the post-hydrolysis state *EcBcsZ*(E55Q)_{CPT}. The cellooligosaccharides and the residues are represented as sticks and lines, respectively. (b) Schematic diagram of the motion of the GH8 endo- β -1,4-glucanase residues during the reaction process. The glutamate and arginine of interest are represented as orange and blue sticks, respectively. When the sugar units interact with the glutamate and/or arginine, the solid circles are in the same color as the glutamate and/or arginine.

bound structure, unlike previous studies. The *EbBcsZ* (D242A)_{CPT} structure provides a novel snapshot of the reaction state, in which two β -1,4-glucan chains lying in subsites -1 to -4 and $+1$ to $+2$ are separated. The distance between the C1 atom of G_{-1} and the 4-OH of G_{+1} is approximately 3 Å, which is longer than the typical length of a C—O single bond (1.43 Å). Thus, *EbBcsZ*(D242A)_{CPT} represents the ‘post-cleavage state’, with G_{-1} in a distorted 5S_1 conformation, immediately after the scissile-bond cleavage (Fig. 5*a*, iii).

The residues Glu54 and Arg245 in *EbBcsZ*(D242A)_{CPT} differed in orientation compared with the corresponding residues in *EcBcsZ*(E55Q)_{CPT} (E55Q and Arg246) and *CtCelA*(E95Q)_{CPT} (E95Q and Arg281). Similar to the reactive state [*CtCelA*(E95Q)_{CPT}] and the post-hydrolysis state [*EcBcsZ*(E55Q)_{CPT}], the side chain of the acid catalyst Glu54 was located between G_{+1} and G_{-1} in the post-cleavage state [*EbBcsZ*(D242A)_{CPT}] (Fig. 5*a*, ii–iv). However, comparison between *EbBcsZ*(D242A)_{CPT} and *EcBcsZ*_{apo} indicated that when the substrate binds, the Glu54 side chain would simultaneously flip and interact with Tyr330 and Arg245 to avoid a clash with the 3-OH of G_{-1} (Figs. 3*b* and 5*a*, i). Thus, upon substrate binding, the acid catalyst side chain flips and keeps this conformation, while the cellooligosaccharide occupies subsite -1 . In the resting state (*EcBcsZ*_{apo}), the N^{H1} atom of Arg246 forms a salt bridge to the O^{H2} atom of Asp116 and was distant from the binding subsites (Fig. 5*a*, i). In the reactive state [*CtCelA*(E95Q)_{CPT}], the corresponding Arg281 was distant from Asp152 and shifted to interact with G_{-1} (Fig. 5*a*, ii). In the post-cleavage state [*EbBcsZ*(D242A)_{CPT}], Arg245 presented two conformations: Arg245_{conf2} was the same as that of the corresponding Arg281 of *CtCelA* in the reactive state, whereas Arg245_{conf1} shifted to interact with G_{+1} (Figs. 3*b* and 5*a*, iii). In the post-hydrolysis state [*EcBcsZ*(E55Q)_{CPT}], Arg246 returned to interact with Asp116 and was distant from subsite $+1$ (Fig. 5*a*, iv). Therefore, this arginine residue has an important role in tethering the cleaved β -1,4-glucan chains. Based on these findings, we summarized a series of conformational changes in the catalytic process of GH8 endo- β -1,4-glucanase to illustrate the whole catalytic mechanism (Fig. 5*b*). The flexibility of the arginine residue allows the post-cleavage state to be captured. The superimposed structures of *EbBcsZ*(D242A)_{CPT} and *EbBcsZ*_{GOL} clearly showed that the side chain of Asp242 does not sterically hinder the conformational changes of G_{-1} and Arg245 (Supplementary Fig. S6). Considering the reaction mechanism of an inverting glycoside hydrolase (Fig. 1), the acid catalyst mutation prevents the formation of the transition intermediate, and the 5S_1 conformation is invisible. The base catalyst activates a water molecule for a nucleophilic attack on the C1 atom of G_{-1} and does not directly attack G_{-1} . Even though the base catalyst is mutated, the reaction may proceed by the very weak nucleophilicity of water. Indeed, previous studies demonstrated that mutating the base catalyst drastically reduced, but did not completely remove, the activity of GH8 enzymes (Fowler *et al.*, 2018; De Vos *et al.*, 2006; Collins *et al.*, 2005). The structural comparison of G_{-1} in the post-cleavage state 5S_1 [*EbBcsZ* (D242A)_{CPT}] with the substrate state β - C_1 [the other glucosyl

unit in *EbBcsZ*(D242A)_{CPT}] and the transition state ${}^{2,5}B$ [*CtCelA*(E95Q)_{CPT}] clearly showed the difference in planarity of G_{-1} (Supplementary Fig. S3*c*). The boat ${}^{2,5}B$ conformer changes to a skew-boat 5S_1 conformer, indicating that the hydrolysis reaction of GH8 enzymes precedes via an unstable conformation to meet the requirements of an antiperiplanar lone-pair hypothesis (Nerinx *et al.*, 2005).

In the structure of *EbBcsZ*(D242A)_{CPT}, we obtained electron density for six glucosyl units in monomers *A–C* as shown in Fig. 3(*a*), although we utilized cellopentaose. Considering that no electron density appeared at subsite -1 in monomer *D* and the electron density for G_{-1} in monomers *A–C* clearly showed the 5S_1 conformation, the electron density might be derived from a mixture of the post-cleavage state of cellopentaose in subsites -3 to $+2$ and cleaved cellotriose in subsites -4 to -2 , but not noncleaved cellopentaose in subsites -4 to $+1$. Combining the binding of oligosaccharides in the structure of *EbBcsZ*(D242A)_{CPT} with a previous thin-layer chromatography (TLC) analysis (Sunagawa *et al.*, 2012), we proposed the binding patterns of oligosaccharides in the trimming mechanism of BcsZ (Fig. 6). The structure shows that *EbBcsZ* has six subsites, -3 to $+2$ and additionally -4 , for binding the β -1,4-glucan chain. The TLC analysis demonstrated

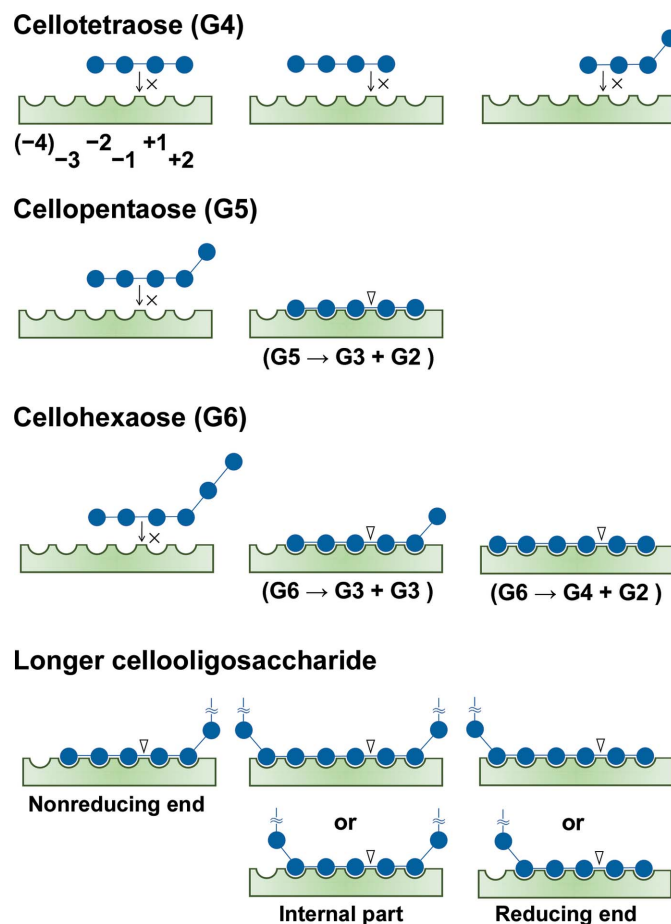


Figure 6
 Schematic diagram of the proposed binding patterns of oligosaccharides in BcsZ. The β -1,4-glucan chains cellotetraose (G4), cellopentaose (G5), cellohexaose (G6) and longer cellooligosaccharides are represented as solid spheres connected by lines. The triangle indicates the scissile bond.

that *EbBcsZ* degrades cellopentaose into cellobiose and cellotriose but does not degrade cellotetraose. Thereby, five cellopentaose glucosyl units should lie in subsites -3 to $+2$ and not in subsites -4 to $+1$ or in the four subsites -2 to $+2$ (Fig. 6, G4 and G5). The TLC analysis also showed that *EbBcsZ* degrades cellohexaose into two cellotrioses or into cellobiose and cellotetraose. Cellohexaose needs to have five glucosyl units in subsites -3 to $+2$ and a free glucosyl unit to produce two cellotrioses. The six glucosyl units of cellohexaose need to be in subsites -4 to $+2$ (Fig. 6, G6) to obtain cellobiose and cellotetraose. Consequently, *EbBcsZ* hydrolyzes cellopentaose or longer cellooligosaccharides when the β -1,4-glucan chain occupies at least subsites -3 to $+2$ (Fig. 6, bottom). Moreover, considering that glycerol molecules preferentially bind to subsites -2 to $+1$ in the *EbBcsZ*_{GOL} structure (Supplementary Fig. S3c), the sugar units in subsites -3 and $+2$ might have a relatively lower affinity than those in subsites -2 to $+1$. Therefore, subsites -3 and $+2$ assist in binding the β -1,4-glucan chain.

5. Conclusion

This work demonstrated that the GH8 endo- β -1,4-glucanase *EbBcsZ* partly degrades gelatinous BC, implying that it plays a potential role in the quality control of BCs. Unlike previous studies, we obtained the *EbBcsZ*(D242A)_{CPT} structure using a base-catalyst mutant, revealing a 5S_1 intermediate as the ‘post-cleavage state’. By comparing GH8 endo- β -1,4-glucanase snapshots, we provided insights into the motion of the residues coupled to the conformational change of the glucosyl unit in subsite -1 during the reaction process. Moreover, based on structural analysis of *EbBcsZ*(D242A)_{CPT}, we proposed a β -1,4-glucan-trimming mechanism for *EbBcsZ* to enhance the understanding of the biosynthesis of high-quality cellulose by bacteria, and our findings open up a route to a deep understanding of the enzymology of glycoside hydrolases.

Acknowledgements

We thank the beamline staff of the Photon Factory and SPring-8 for their technical assistance during X-ray diffraction data collection (Proposal Nos. 2018B2508, 2019B2537 and 2021A2756).

Funding information

This work was supported in part by a Grant-in-Aid for Scientific Research (A) (No. 21H01754 to MY) from the Ministry of Education, Culture, Sports, Science and Technology of Japan, and also by Platform Project for Supporting Drug Discovery and Life Science Research [Basis for Supporting Innovative Drug Discovery and Life Science Research (BINDS)] from Japan Agency for Medical Research and Development (AMED) under Grant Numbers JP18am0101071 and JP19am0101083.

References

- Acheson, J. F., Derewenda, Z. S. & Zimmer, J. (2019). *Structure*, **27**, 1855–1861.
- Ahmad, I., Rouf, S. F., Sun, L., Cimdins, A., Shafeeq, S., Le Guyon, S., Schottkowski, M., Rhen, M. & Römling, U. (2016). *Microb. Cell Fact.* **15**, 177.
- Ardèvol, A. & Rovira, C. (2015). *J. Am. Chem. Soc.* **137**, 7528–7547.
- Chen, V. B., Arendall, W. B., Headd, J. J., Keedy, D. A., Immormino, R. M., Kapral, G. J., Murray, L. W., Richardson, J. S. & Richardson, D. C. (2010). *Acta Cryst.* **D66**, 12–21.
- Chundawat, S. P. S., Beckham, G. T., Himmel, M. E. & Dale, B. E. (2011). *Annu. Rev. Chem. Biomol. Eng.* **2**, 121–145.
- Cockburn, D. & Svensson, B. (2013). *Carbohydr. Chem.* **39**, 204–221.
- Cockburn, D., Wilkens, C., Dilokpimol, A., Nakai, H., Lewińska, A., Abou Hachem, M. & Svensson, B. (2016). *PLoS One*, **11**, e0160112.
- Collins, T., De Vos, D., Hoyoux, A., Savvides, S. N., Gerday, C., Van Beeumen, J. & Feller, G. (2005). *J. Mol. Biol.* **354**, 425–435.
- Cremer, D. & Pople, J. A. (1975). *J. Am. Chem. Soc.* **97**, 1354–1358.
- Cuyvers, S., Dornez, E., Delcour, J. A. & Courtin, C. M. (2011). *Appl. Microbiol. Biotechnol.* **92**, 539–549.
- Cuyvers, S., Dornez, E., Delcour, J. A. & Courtin, C. M. (2012). *Crit. Rev. Biotechnol.* **32**, 93–107.
- Czaja, W., Krystynowicz, A., Bielecki, S. & Brown, R. M. Jr (2006). *Biomaterials*, **27**, 145–151.
- Czaja, W., Romanovicz, D. & Brown, R. M. Jr (2004). *Cellulose*, **11**, 403–411.
- De Vos, D., Collins, T., Nerinckx, W., Savvides, S. N., Claeysens, M., Gerday, C., Feller, G. & Van Beeumen, J. (2006). *Biochemistry*, **45**, 4797–4807.
- Emsley, P., Lohkamp, B., Scott, W. G. & Cowtan, K. (2010). *Acta Cryst.* **D66**, 486–501.
- Fowler, C. A., Hemsworth, G. R., Cuskin, F., Hart, S., Turkenburg, J., Gilbert, H. J., Walton, P. H. & Davies, G. J. (2018). *Acta Cryst.* **D74**, 946–955.
- Fujiwara, T., Komoda, K., Sakurai, N., Tajima, K., Tanaka, I. & Yao, M. (2013). *Biochem. Biophys. Res. Commun.* **431**, 802–807.
- Guérin, D. M., Lascombe, M. B., Costabel, M., Souchon, H., Lamzin, V., Béguin, P. & Alzari, P. M. (2002). *J. Mol. Biol.* **316**, 1061–1069.
- Helenius, G., Bäckdahl, H., Bodin, A., Nannmark, U., Gatenholm, P. & Risberg, B. (2006). *J. Biomed. Mater. Res.* **76A**, 431–438.
- Hu, S.-Q., Gao, Y.-G., Tajima, K., Sunagawa, N., Zhou, Y., Kawano, S., Fujiwara, T., Yoda, T., Shimura, D., Satoh, Y., Munekata, M., Tanaka, I. & Yao, M. (2010). *Proc. Natl Acad. Sci. USA*, **107**, 17957–17961.
- Kabsch, W. (2010). *Acta Cryst.* **D66**, 125–132.
- Kawano, S., Tajima, K., Kono, H., Numata, Y., Yamashita, H., Satoh, Y. & Munekata, M. (2008). *J. Biosci.* **106**, 88–94.
- Kawano, S., Tajima, K., Uemori, Y., Yamashita, H., Erata, T., Munekata, M. & Takai, M. (2002). *DNA Res.* **9**, 149–156.
- Koo, H. M., Song, S. H., Pyun, Y. R. & Kim, Y. S. (1998). *Biosci. Biotechnol. Biochem.* **62**, 2257–2259.
- Koshland, D. E. (1953). *Biol. Rev.* **28**, 416–436.
- Krissinel, E. & Henrick, K. (2004). *Acta Cryst.* **D60**, 2256–2268.
- Lee, K.-Y., Buldum, G., Mantalaris, A. & Bismarck, A. (2014). *Macromol. Biosci.* **14**, 10–32.
- Lee, S. E. & Park, Y. S. (2017). *Mol. Cell. Toxicol.* **13**, 257–261.
- Liebschner, D., Afonine, P. V., Baker, M. L., Bunkóczi, G., Chen, V. B., Croll, T. I., Hintze, B., Hung, L.-W., Jain, S., McCoy, A. J., Moriarty, N. W., Oeffner, R. D., Poon, B. K., Prisant, M. G., Read, R. J., Richardson, J. S., Richardson, D. C., Sammito, M. D., Sobolev, O. V., Stockwell, D. H., Terwilliger, T. C., Urzhumtsev, A. G., Videau, L. L., Williams, C. J. & Adams, P. D. (2019). *Acta Cryst.* **D75**, 861–877.
- Mazur, O. & Zimmer, J. (2011). *J. Biol. Chem.* **286**, 17601–17606.
- Morgan, J. L. W., McNamara, J. T., Fischer, M., Rich, J., Chen, H.-M., Withers, S. G. & Zimmer, J. (2016). *Nature*, **531**, 329–334.

- Morgan, J. L. W., Strumillo, J. & Zimmer, J. (2013). *Nature*, **493**, 181–186.
- Nakai, T., Sugano, Y., Shoda, M., Sakakibara, H., Oiwa, K., Tuzi, S., Imai, T., Sugiyama, J., Takeuchi, M., Yamauchi, D. & Mineyuki, Y. (2013). *J. Bacteriol.* **195**, 958–964.
- Nerinckx, W., Desmet, T., Piens, K. & Claeysens, M. (2005). *FEBS Lett.* **579**, 302–312.
- Nishi, Y., Uryu, M., Yamanaka, S., Watanabe, K., Kitamura, N., Iguchi, M. & Mitsuhashi, S. (1990). *J. Mater. Sci.* **25**, 2997–3001.
- Nogi, M. & Yano, H. (2008). *Adv. Mater.* **20**, 1849–1852.
- Nojima, S., Fujishima, A., Kato, K., Ohuchi, K., Shimizu, N., Yonezawa, K., Tajima, K. & Yao, M. (2017). *Sci. Rep.* **7**, 13018.
- Pang, J., Wang, J., Liu, Z., Zhang, Q. & Qi, Q. (2019). *BMC Biotechnol.* **19**, 63.
- Petersen, L., Ardèvol, A., Rovira, C. & Reilly, P. J. (2009). *J. Phys. Chem. B*, **113**, 7331–7339.
- Römling, U. & Galperin, M. Y. (2015). *Trends Microbiol.* **23**, 545–557.
- Ross, P., Mayer, R. & Benziman, M. (1991). *Microbiol. Rev.* **55**, 35–58.
- Schramm, M. & Hestrin, S. (1954). *J. Gen. Microbiol.* **11**, 123–129.
- Shah, J. & Brown, R. M. Jr (2005). *Appl. Microbiol. Biotechnol.* **66**, 352–355.
- Somerville, C. (2006). *Annu. Rev. Cell Dev. Biol.* **22**, 53–78.
- Standal, R., Iversen, T. G., Coucheron, D. H., Fjaervik, E., Blatny, J. M. & Valla, S. (1994). *J. Bacteriol.* **176**, 665–672.
- Sunagawa, N., Tajima, K., Hosoda, M., Kawano, S., Kose, R., Satoh, Y., Yao, M. & Dairi, T. (2012). *Cellulose*, **19**, 1989–2001.
- Torgbo, S. & Sukyai, P. (2020). *Polym. Degrad. Stabil.* **179**, 109232.
- Wong, H. C., Fear, A. L., Calhoon, R. D., Eichinger, G. H., Mayer, R., Amikam, D., Benziman, M., Gelfand, D. H., Meade, J. H., Emerick, A. W., Bruner, R., Ben-Bassat, A. & Tal, R. (1990). *Proc. Natl Acad. Sci. USA*, **87**, 8130–8134.
- Yamanaka, S., Watanabe, K., Kitamura, N., Iguchi, M., Mitsuhashi, S., Nishi, Y. & Uryu, M. (1989). *J. Mater. Sci.* **24**, 3141–3145.
- Yasutake, Y., Kawano, S., Tajima, K., Yao, M., Satoh, Y., Munekata, M. & Tanaka, I. (2006). *Proteins*, **64**, 1069–1077.